Atmos. Meas. Tech. Discuss., 3, 4645–4674, 2010
www.atmos-meas-tech-discuss.net/3/4645/2010/
doi:10.5194/amtd-3-4645-2010

Atmospheric
Measurement
Techniques
Discussions

Rapid methods for inversion of MAXDOAS elevation profiles to surface-associated box concentrations, visibility, and heights: application to analysis of Arctic BrO events

D. Donohoue[1,*], **D. Carlson**[2], **and W. R. Simpson**[1,2]

[1]Geophysical Institute, University of Alaska Fairbanks, Fairbanks, AK 99775, USA
[2]Department of Chemistry and Biochemistry, University of Alaska Fairbanks, Fairbanks, AK 99775-6160, USA
[*]now at: University of East Anglia, School of Environmental Sciences, Norwich, NR4 7TJ, UK

Received: 11 September 2010 – Accepted: 5 October 2010 – Published: 1 November 2010

Correspondence to: W. R. Simpson (wrsimpson@alaska.edu)

Published by Copernicus Publications on behalf of the European Geosciences Union.

Abstract

Multiple Axis Differential Optical Absorption Spectroscopy (MAXDOAS) is a remote sensing technique that measures surface-associated trace gas profiles using simple automated instrumentation that requires very low power and is deployable at remote sites. However, the analysis of MAXDOAS data is complex and often cannot be applied rapidly or consistently over long measurement periods. Here we present three transparent methods to analyze MAXDOAS data. The box profile method finds the best trace gas layer height and surface-associated vertical column density (VCD) to simultaneously fit oxygen collisional dimer (O_4) and trace gas differential slant column density (dSCD) observations. The elevated viewing method estimates the surface-associated VCD from observations at high view elevations, such as 10° and 20°. The horizon viewing method estimates the surface concentration of a trace gas by using near-horizon view trace gas and O_4 data. We apply these methods to a two-month data set and show that the methods retrieve information 80% of the time and provides a consistent time series. Surface-associated trace gas VCD observations by the elevated viewing method correlate ($r^2>0.93$) with the box profile method with slopes within 15% of unity. Surface-associated concentration observations from the horizon viewing method correlate well ($r^2>0.90$) with the box profile method and a slope within 4% of unity. Application of these retrieval methods to UV-absorbing trace gases other than BrO is straightforward, and application in other spectral regions is discussed. These methods provide rapid and comprehensive inversions of MAXDOAS spectral data that are useful during field campaigns, as well as, verification of more complex (e.g. optimal estimate inversion) methods.

1 Introduction

Variations of Differential Optical Absorption Spectroscopy (DOAS) have been used to study trace gases constituents in the atmosphere since the late 1920s (Dobson and

Harrison, 1926). Numerous atmospheric trace gases have been detected using the DOAS technique, including O_3, NO_2, BrO, OClO, SO_2, HCHO, CHOCHO, and H_2O (e.g., Afe et al., 2004; Hausmann and Platt, 1994; Hebestreit et al., 1999, Wittrock et al., 2000). Active DOAS techniques use artificial light sources to measure averaged trace gas concentrations along a defined path. In this manuscript, we consider passive MAXDOAS spectroscopy, which involves more data analysis but benefits from not needing an external light source and can be used to remotely sense trace gas vertical profiles (e.g., Hönninger et al., 2004a).

In general, the MAXDOAS technique requires the collection of quality spectra at differing viewing geometries, the conversion of these spectra to differential slant column densities (dSCD) of trace gases between the views, and modeling of trace gas profiles consistent with these differential slant column densities. Two desirable properties of the derived trace gas profiles are the surface-associated vertical column densities (SA-VCD) and the surface trace gas concentration. As we demonstrate below, MAXDOAS has sensitivity to trace gases in the lowest few kilometers of the atmosphere above the observing location's altitude, so by the SA-VCD, we mean the partial VCD in the lowest few kilometers of the atmosphere. While the first two steps of MAXDOAS analysis are relatively well characterized and there is some uniformity in their application, the methods used to convert dSCDs to SA-VCDs and surface trace gas species concentrations vary greatly between studies. One of the most common approaches is to first filter the data to include only clear sky days. Once clear sky days have been identified, a simple geometric approximation is used to calculate airmass factors. Differential airmass factors (dAMF) are the ratio between an observed dSCD at a specific view elevation and the SA-VCD. The dAMFs are used to convert dSCDs to SA-VCDs. After a SA-VCD is determined a standard vertical profile is assumed, such as uniform mixed layer to 1 ± 0.5 km. Using this assumed profile the SA-VCDs are converted to estimated trace gas concentrations (Hönninger and Platt, 2002; Hönninger et al., 2004b,c; Leser et al., 2003). The second method is similar to the first; however, rather than using the geometric approximation to derive SA-VCD, radiative transfer models, such as SCIATRAN (Rozanov et al., 2005) or TRACY-II (Deutschmann and Wagner, 2007), are used to calculate differential airmass factors (Lee et al., 2008). Radiative transfer models (RTM) require some assumptions, specifically concerning the vertical profiles, visibility, solar zenith angle, solar azimuth and albedo. Therefore, studies that employ RTMs inherently make assumptions concerning the atmospheric conditions. Again the data are usually filtered to include only clear sky days, the calculated *d*AMFs are used the determine SA-VCDs for the trace gas species. These methods have two major disadvantages. First, the clear sky filter greatly reduces the number of measurements and the conditions under which trace gases are monitored. Second, choosing a fixed vertical profile requires a series of assumptions concerning the state of the atmosphere (the trace gas vertical profile and visibility conditions). These assumptions are not appropriate for an entire campaign or across platforms, as the atmospheric conditions are not fixed. So while these methods have the advantage of clearly defined assumptions they are limited in that one set of assumptions is only applicable to a limited data set.

These two methods have been extended to include non-clear sky conditions by applying fixed visibility conditions or by using the observed *d*SCDs of O_4 to define the visibility profile (Wagner et al., 2004) prior to applying a fixed trace gas profile (Leigh et al., 2007; Sinreich et al., 2007; Wittrock et al., 2004). While this method has the advantage of extending the retrieval to non-clear sky days, the trace gas profile is still fixed and has the same disadvantages as discussed with the first two methods. In order to overcome this disadvantage, a recent study (Li et al., 2010) presented a method to systematically characterize the visibility conditions using three free visibility parameters: total aerosol extinction, the fraction of aerosol in the surface layer, and the aerosol layer height. During this study it was found that these parameters correlated well with locally measured aerosol extinction, and resulted in reasonable aerosol layer heights.

On the other extreme, the optimal estimation inversion method (Rodgers, 1976) was developed to account for the highly variable atmosphere. The method focuses on determining the atmosphere that is the best solution from all the possible solution that is consistent with the observations (Frieß et al., 2006; Heckel et al., 2005). The method gives an optimal inversion of the data, but may over-interpret small, or even noise, features in the observations giving an overly complex result or inconsistent profiles through time.

In this work, we developed three transparent analysis methods that give robust and consistent results across a variety of atmospheric visibility conditions. These rapid methods can be used either during field campaigns for first looks at the data or as a basis for/verification of more involved optimal estimation analysis. In the first of these methods, which we call "box profile fitting", we used the TRACY-II RTM to obtain *d*AMFs for a series of potential box profiles with varying layer heights and visibility parameters. MAXDOAS observations of O_4 and a trace gas of interest are then fitted to the best combination of layer height and visibility conditions to give the best "box profile" for that trace gas. Because this method derives a SA-VCD and a layer thickness, we can calculate the concentration of the trace gas in the box. A second method, called the "horizon view" method, uses low elevation spectra to calculate the surface concentration of the trace gas directly by deriving an effective pathlength, from the O_4 data, and simply divides the trace gas slant column density by this effective pathlength. The third method, called the "elevated viewing" method, calculates the SA-VCD by using *d*SCD observations at moderately high elevations (e.g. 10° or 20°). It is shown that these three methods are generally consistent for a two-month data time series. These methods have the advantages of being applicable over a large range of observations (over an entire campaign, between campaigns, for different trace gas species), as well as, having well-defined assumptions that can be directly compared to observations.

2 Methods

2.1 Instrument description

The MAXDOAS instrument used in this work was designed as a low power, no maintenance instrument that could be deployed in extreme environments, such as the Arctic. Full details on the design and benefits of this system can be found in a Carlson et al. (2010). Details on the incorporation of this instrument into a remote buoy system can be found in Knepp et al. (2010). The instrument used in this study shared the same telescope elevation scan device, but used a higher-quality spectrometer (an Ocean Optics QE65000) than the buoy system.

2.2 Reference spectrum selection methods

The MAXDOAS method requires selection of an appropriate reference spectrum. The *d*SCDs are quantified with respect to this reference, which has by definition zero *d*SCDs for all absorbers. Solar light possesses strong Fraunhofer features due to absorption by atoms in the sun that can mask the weaker atmospheric trace gas absorptions. The selection of a proper Fraunhofer reference spectrum is essential to obtaining good results and plays a role in defining the region in which the instrument is most sensitive. In this work, we calculated differential slant column densities using two referencing methods.

In selecting a referencing method, there must be a balance between capturing atmospheric fluctuations and removing instrument variations. The first type of reference uses a daily zenith reference, DZ-MAXDOAS, which means the Fraunhofer reference for each day is the zenith spectra collected at solar noon, $\mathrm{FRS}_{\mathrm{DZ}}$. This type of referencing will capture diurnal variations while removing any daily instrumental variations (e.g. slow temperature fluctuations or instrumental degradation). From these data we can apply both a twilight zenith scattered light analysis to obtain stratospheric trace gas abundances and a MAXDOAS analysis after a subtraction of the zenith *d*SCD collected at nearly the same time as a measurement to obtain surface associated *d*SCDs. A disadvantage of this method is that large differential features from stratospheric absorbers such as ozone need to be fitted very accurately so that the resulting residuals do not affect weaker trace gas absorption features. Since the ozone absorption spectrum is a function of temperature, ozone absorption spectra at two temperatures were included. It should be noted that covariance between these spectra can give non-physical results.

The second analysis procedure uses a local, or concurrent, zenith reference, LZ-MAXDOAS; this means the zenith reference used is collected at the same time as all other elevation angles, FRS_{LZ}. By using the local or concurrent zenith reference as the Fraunhofer reference spectrum, virtually all the instrumental variations, any long term trends in the data, and any variations due to changes in the trace gases above ~2 km were removed from the measurement. This method is preferred for MAXDOAS analysis of tropospheric trace gases. The primary disadvantage of the LZ-MAXDOAS method is that it does not provide any information on daily or seasonal variations in the trace gas abundances nor does it provide information on abundances above the troposphere.

2.3 Conversion of spectra to differential slant column densities

In this work, we fit spectral data based on the suggestions from the intercomparison done by Aliwell et al. (2002) using the QDOAS least-squares fitting program (Fayt and Van Roozendael, 2001). We have minor changes from Aliwell et al. (2002) as described below. An overview of our fitting scenarios can be found in Table 1. Aliwell et al. (2002) suggest fitting the region from 346 to 359 nm, but we extended the long wavelength limit of the fitting window to 364 nm to include the small O_4 peak around 360 nm, as well as, the third BrO peak at 360.5 nm. A spectrum of the isolated 334 nm emission from a low-pressure mercury lamp (Pen Ray Corporation) was used as the averaging kernel (instrumental spectral slit function). The averaging kernel was close to Gaussian in shape and had a 0.6 nm full width at half maximum. Spectra were wavelength corrected using a solar spectrum from Kitt Peak (Kurucz et al., 1984). Vacuum to air wavelength corrections were made using the Edlén equation (Birch and Downs, 1993). A fixed ring spectrum was calculated for a zenith spectrum collected on a clear sky day using the DOASIS software. We used the best available cross-section data, hence we updated the Aliwell (2002) recommended fitting scenario with more recent cross-sections for O_4 (Hermans et al., 2001) and O_3 (Bogumil, 2000), eliminating some concerns due to shift and stretch. This fitting method produced similar differential slant column densities to the unaltered Aliwell et al. (2002) fitting scenario but resulted in a reduced residual. The DZ-MAXDOAS fitting method includes ozone spectra at two temperatures to account for ozone absorption at stratospheric and tropospheric temperatures, but we found that the LZ-MAXDOAS method only required one ozone spectrum because the LZ referencing method is more effectively removing stratospheric influences, which are large for ozone due to its prevalence in that layer.

Figure 1 shows fits for 14 March 2008, 02:09 UTC at a view elevation of 3° from the horizon. Panel a is the DZ-MAXDOAS fitting; from this plot we see the signature from stratospheric O_3 and NO_2. While in panel b, LZ-MAXDOAS fitting, we see that these O_3 and NO_2 signals are reduced by the referencing method. On the other hand we see that the BrO derived from both methods is similar because of the large sensitivity of MAXDOAS to surface-associated trace gases when viewing at low elevations above the horizon. A resulting time series of the BrO *d*SCDs for both fitting scenarios is shown in Fig. 2. Once again the differences in the fitting scenarios are evident. The DZ-MAXDOAS fitting demonstrates the expected pattern in that all elevation angles track the *d*SCD determined at the zenith. These zenith determinations show the expected increase in BrO *d*SCD toward both twilight periods resulting in a U-shaped diurnal profile. A secondary analysis of the DZ-MAXDOAS twilight data could be done to characterize stratospheric layer abundances (e.g., see Aliwell et al., 2002). At the other elevation angles, using both referencing methods, the observed BrO *d*SCDs increase as view elevations decrease. This observation is only consistent with a significant amount of BrO being present near the surface, as demonstrated below.

As a final validation of the derived dSCDs at non-zenith view elevations from both the DZ-MAXDOAS fitting and the LZ-MAXDOAS fitting were compared. To compare dSCDs obtained at non-zenith view elevation, the DZ-MAXDOAS data require subtraction of the local zenith dSCD. As expected, the two methods obtain similar dSCDs with a slope near unity, 0.978, and a high r^2 of 0.998.

2.4 Airmass factor calculations and profile sensitivity

The airmass factor (AMF) is the ratio of the slant column density to the vertical column density along a certain view elevation, α; thus the airmass factor is

$$\mathrm{AMF}(\alpha) = \frac{\mathrm{SCD}(\alpha)}{\mathrm{SA-VCD}}. \tag{1}$$

Note that we only use profiles containing surface-associated trace gases, so the total VCD in the modeled profiles is equal to the SA-VCD. We reference all spectra to the local (same time) zenith spectrum and observe dSCDs compared to this reference. Thus, we can expand Eq. (1) to the differential airmass factor

$$d\mathrm{AMF}(\alpha) = \mathrm{AMF}(\alpha) - \mathrm{AMF}(90^\circ) = \frac{\mathrm{SCD}(\alpha) - \mathrm{SCD}(90^\circ)}{\mathrm{SA-VCD}} = \frac{d\mathrm{SCD}(\alpha)}{\mathrm{SA-VCD}} \tag{2}$$

The calculation of the air mass factor was performed using the 3-D full spherical Monte Carlo radiative transfer model “TRACY-II”. All airmass factors were calculated assuming a solar zenith angle of 70°, a solar azimuth of 180°, an albedo of 0.9, an instrumental angle of acceptance of 1°, and a detector height of 10 m. Airmass factors for other solar zenith and azimuth angles were compared and found to have a minor effect, as has been noted (Hönninger et al., 2004a; Wagner et al., 2007). A box profile with two parameters, layer height and surface concentration, was used as the assumed vertical profile for the trace gas of interest (e.g. BrO). The visibility conditions were set using a single aerosol extinction coefficient in a layer with the same height as the trace gas box profile.

Figure 3 is a plot of the relative sensitivities of the ground-based MAXDOAS measurement using a series of potential box profiles. Each box is 500 m thick and contains a BrO SA-VCD of 3×10^{13} molecules cm^{-2} assuming a visibility of 20 km. Figure 3 panel a plots the expected *d*SCD versus elevation angle. It is evident that in order to produce significant *d*SCDs BrO at the lowest elevation angles (1°, 2°, and 3°) BrO must be present in the lowest 500 m of the atmosphere. Figure 3 panel b shows the *d*SCD BrO produced in each 500 m box discussed above at three specific elevation angles (2°, 10°, and 20°). Here we see two important trends. First, lower view elevation spectra (2°) are more sensitive to BrO near the surface, while higher view elevation (10° and 20°) observations are less sensitive to BrO overall. Second, the higher view elevations are also less sensitive to the exact location (altitude) of the BrO layer, while if there is not BrO in the lowest 500 m of the atmosphere lower elevation *d*SCD will be comparatively small. Thus, *d*SCD observations at higher elevation angles are a more direct method of measuring the SA-VCD of BrO.

2.5 Box profile fitting method

To determine the best surface-based box profile for each set of MAXDOAS measurements, airmass factors were calculated for ninety potential box profiles, and a fitting procedure was used to select the best profile using the combination of trace gas (e.g. BrO) *d*SCD versus elevation profiles and O_4 *d*SCD versus elevation profiles. The airmass factors were generated by producing all combinations of the following conditions: nine aerosol extinction (AE) values, 0.01, 0.05, 0.1, 0.2, 0.4, 0.6, 0.8, 1, and 2 (km^{-1}) and ten layer heights (Z), 100, 300, 500, 700, 1000, 1200, 1400, 1600, 1800 and 2000 (m).

Using these *d*AMF, an estimated SA-VCD (SA-VCD$_{EST}$) for each potential box profile was calculated for both the trace gas species and the oxygen dimer,

$$\mathrm{SA-VCD_{EST}} = \frac{\sum_i d\mathrm{SCD}(\alpha_i)}{\sum_i d\mathrm{AMF}(\alpha_i)}. \tag{3}$$

In Eq. (3), there are n observation angles, taken from the set $\{a_i\}$, typically $\{1^\circ, 2^\circ, 3^\circ, 5^\circ, 10^\circ, 20^\circ\}$. The SA-VCD$_{\mathrm{EST}}$ is simply the average observed dSCD divided by the average dAMF for that assumed box profile. These SA-VCD$_{\mathrm{EST}}$ show the potential range of SA-VCDs calculated for a given MAXDOAS profile, Fig. 4. In panel a, we see that the derived SA-VCD$_{\mathrm{EST}}$ for the trace gas species follows contours which are the product of the visibility and height parameters. This finding was expected as the observed trace gas SA-VCD depends upon both on the observed path length (visibility) and the distribution of the trace gas species (layer height). As the visibility decreases the average path length also decreases, this truncated path length reduces the differences observed between lower (2°) and higher (20°) view elevations. Additionally, as the layer of trace gas becomes thicker the difference between the observed trace gas dSCD at view elevation close to the horizon (2°) and those observed at higher view elevations (20°) decreased. In panel b, we see that the O_4 SA-VCD$_{\mathrm{EST}}$ contours tend to only follow the visibility parameter and were insensitive to layer height. This finding is expected as the O_4 concentration is independent of the height of the boundary layer and exponentially decreases with height. Thus the observed O_4 dSCD depend strongly on the average path length of the measurement. Therefore, as visibility decreases, the average path length of the instrument decreases and the observed O_4 dSCD also decrease. Thus, by simultaneously fitting both of O_4 and the trace gas species a "best fit" box profile can be selected from the potential profiles. Finally, it should also be noted that the calculated O_4 SA-VCD$_{\mathrm{EST}}$ reach unrealistic values, 4×10^{43} molecules^2 cm^{-5}. These values are evidence that we have employed an inappropriate box model, as the derived O_4 SA-VCD$_{\mathrm{EST}}$ is inconsistent with the known O_4 concentration in the atmosphere; therefore, the O_4 SA-VCD$_{\mathrm{EST}}$ was employed as a limit later in this analysis.

To identify this best fit box profiles a simple RMS analysis was used. This RMS analysis aims to match the relative shape of the MAXDOAS elevation profile data by individually comparing each observation to a modeled elevation profile. The calculated differential slant column densities, $d\mathrm{SCD}_{\mathrm{CALC}}(a_i)$, were determined for each elevation angle using the ninety potential profiles, Eq. (4).

$$d\mathrm{SCD}_{\mathrm{calc}}(\alpha_i) = \mathrm{SA-VCD}_{\mathrm{EST}} \times d\mathrm{AMF}(\alpha_i) \quad (4)$$

These $d\mathrm{SCD}_{\mathrm{CALC}}(a_i)$ were then compared to the observed $d\mathrm{SCD}_{\mathrm{OBS}}(a_i)$ using a root mean square (RMS) deviation analysis.

$$\mathrm{RMS} = \left(\sum_i \left[\frac{(d\mathrm{SCD}_{\mathrm{calc}}(\alpha_i) - d\mathrm{SCD}_{\mathrm{obs}}(\alpha_i))}{\sigma}\right]^2\right) \Big/ n \quad (5)$$

The coefficient of variation, σ, in Eq. (5) was taken to be 1.4×10^{13} molecules cm^{-2} for BrO and 7.1×10^{42} molecules^2 cm^{-5} for O_4. Figure 5 shows the resulting RMS values for the BrO and O_4 in panels a and b, respectively. In this plot, the observed SA-VCD$_{\mathrm{EST}}$ trends are more evident, as there is a single minimum well at specific visibility range in the O_4 plot and a series of minimum wells along the contour of the product of the visibility and layer height parameters in the trace gas plot. To account for both these plots we take the sum of these two RMS, a plot of the resulting total RMS is in Fig. 5 panel c. This plot shows a minimum well for the a single box profile where both the O_4 and trace gas RMS is minimized; this set of layer height and visibility describes the best fit box profile.

As we have identified a best fit box profile for each MAXDOAS measurement, we must also identify times when this box profile was not appropriate. To determine these times we applied a series of limits. First, the O_4 vertical profile is well-defined and therefore the O_4 SA-VCD is well defined, $\sim 1 \times 10^{43}$ molecules^2 cm^{-5}. In Fig. 4, panel b it was evident that the O_4 SA-VCD$_{\mathrm{EST}}$ obtained values an significantly larger, as this is inconsistent with the actual value we applied a filter ($0.8 \times 10^{43} <$ SA-VCD$_{\mathrm{EST}}$

O_4/(molecules^2 cm^{-5}) < 1.3×10^{43}) to ensure that only parameter sets with valid O_4 SA-VCD$_{EST}$ values are considered as a potential fits. We also applied an upper limit of 1.5 to the RMS deviation for both the trace gas species and O_4. If the RMS deviation is larger than 1.5 we assume that the single box profile is insufficient for the characterization of the vertical profile. With these limits we can identify when the one box profile is a valid assumption. The quality of MAXDOAS analysis is highly dependent on the visibility, we characterized the data into one of four cloud classes, with each cloud class having increasing error, based the *d*SCD O_4 at a view elevation of 2°. Since the sensitivity of the technique is decreased with decreasing visibility, all measurement with *d*SCD O_4 below 1.55×10^{43} molecules^2 cm^{-5} (around 5 km visibility) were classified as cloud type IV and not converted to BrO SA-VCDs or BrO concentrations.

The BrO SA-VCD was determined by *d*SCD fitting and the subsequent SA-VCD derivation, therefore the calculation of BrO SA-VCD error must include all errors associated with this process. These errors include the error associated with the determination of the *d*SCD BrO. We determined this for each set of *d*SCD measurements by taking the ratio of the *d*SCD error determined by the QDOAS fitting program and the *d*AMF for BrO by the TRACY-II RTM at 2°. There is also the error in the SA-VCD due to which fitting program was used. We determined this by using the DOASIS, WinDOAS and QDOAS programs to calculated the SA-VCD and found that these programs agreed within 7%. There is a small error associated with determination of the view elevation which was determined to within 1° of the true elevation. This small uncertainty leads to a 3% error in the overall determination of the BrO SA-VCD. One of the largest errors is due to the selection of an appropriate "best fit" box profile for the conversion to BrO SA-VCDs. We determined the magnitude of this error by comparing the SA-VCD derived with the SA-VCDs derived if we step up or step down either parameter. For example if the derived a parameter set of visibility = 0.2 km^{-1} and the layer height = 300 km, we consider the BrO SA-VCD at 0.2 km^{-1} and 100 km, 0.2 km^{-1} and 500 km, 0.4 km^{-1} and 300 km, and 0.1 km^{-1} and 300 km. This comparison leads to an error of 20%. The final error is the error associated with decreasing visibility. As discussed before, as the visibility decrease the sensitivity of the MAXDOAS system also decreases. Therefore, we applied an error to each cloud type: Cloud Type I – 10%, Cloud Type II – 25%, and Cloud Type III – 50%.

2.6 Elevated viewing SA-VCD estimation method

We observed in Fig. 3 panel b that the higher viewing elevation dSCDs given a fixed SA-VCD were more independent of layer height than lower viewing elevations. This effect can be alternatively stated as: the airmass factors for the higher elevation angles are less dependent on the layer elevation. Therefore, the SA-VCD can be derived simply by inversion of Eq. (1) using a single dAMF, which we call $d\text{AMF}_{\text{EV}}$ at higher view elevations. The elevated viewing method $\text{SA-VCD}_{\text{EV}}$ estimate is given by

$$\text{SA}-\text{VCD}_{\text{EV}} = \frac{d\text{SCD}(\alpha)}{d\text{AMF}_{\text{EV}}(\alpha)}. \tag{6}$$

In Eq. (6), only the 10° and 20° viewing angles are used. The $d\text{AMF}_{\text{EV}}$ for these elevated viewing geometries was determined for the ninety potential box profiles ranged from 1.0 to 5.0 with an average of 3.45 at an elevation angle of 10°, and 0.9 to 2.3 with an average of 1.86 at 20°. Because the MAXDOAS method loses sensitivity to trace gases above ~2 km above the surface, these values of effective dAMFs are generally appropriate for boundary layer or other surface-associated trace gases. However, if the trace gas has a more complex vertical profile or is known to exist with large abundances above ~2 km altitude, this method should be used with great caution.

2.7 Horizon viewing surface concentration estimation method

Near horizon views afford the highest sensitivity to surface-associated trace gases, but the observed dSCD is a strong function of visibility. However, as the O_4 dSCD is also strongly dependent upon visibility, the combination of trace gas and O_4 observations can be used to compute surface concentrations of the trace gas directly. Consider a view elevation that is low enough to not escape a surface layer of trace gas of constant concentration over the effective pathlength. In the mid UV (e.g. 340 nm), a typical clear sky visibility is on the order of 12 km, thus for a 2° elevation angle, a 12 km ray traverses from the surface to ~400 m elevation. Often the trace gas concentration will be relatively constant over this altitude range. The actual pathlength can be derived from the assumption that the zenith reference has little absorption as compared to the low elevation views, so we can estimate that the differential slant column density is close to the slant column density, which is equal to the product of the surface concentration times the pathlength. Thus, the horizon view pathlength, L_{HV}, is

$$L_{\mathrm{HV}} = \frac{d\mathrm{SCD}\,\mathrm{O}_4}{[\mathrm{O}_4]_{\mathrm{surf}}}. \tag{7}$$

Note that the cross section for O_4 is typically expressed in terms of the square of the oxygen concentration, which is well determined by surface pressure measurements. Thus, at standard temperature and pressure, $[\mathrm{O}_4]_{\mathrm{surf}}=3.16\times10^{37}$ molecules^2 cm^{-6}. However, the temperature dependence of the $2\mathrm{O}_2\rightleftarrows\mathrm{O}_4$ equilibrium is a subject of debate (Greenblatt et al., 1990; Hermans et al., 1999; Long and Ewing, 1973; Sneep and Ubachs, 2003; Sneep et al., 2006) and to the extent that it is not thermoneutral, there will be a temperature dependence to the effective surface concentration of O_4 as expressed in these units.

Once we obtained an estimated view length we calculated a trace gas concentration estimated by the horizon viewing method,

$$[\text{Trace Gas}]_{\mathrm{HV}} \approx \frac{d\mathrm{SCD}\,\text{Trace Gas}}{L_{\mathrm{HV}}}. \tag{8}$$

The resulting surface trace gas concentration can then be converted to a mixing ratio. In using this method, it is important to realize that the near clear sky pathlength in the UV is a strong function of wavelength due to the prevalence of Rayleigh scattering. Therefore, the O_4 and trace gas dSCDs should be derived in the same spectral region.

For BrO, this condition is easily satisfied, and for NO_2 and other UV absorbers, it can be satisfied by selection of spectral region.

3 Results and discussion

3.1 Box profile fitting results

We applied the one box model, with the aforementioned limits; Fig. 6 is a time series from Barrow, AK form 6 March to 8 June 2008. This plot includes data for the 2 h before and after solar noon, as well as, the overall average for the day at solar noon. From these data, we see that the derived SA-VCDs for this time period, in general, agree within the error limits. This finding is expected, as the changes in BrO tend to occur on the order of a day, thus measurement made with a few hours should have similar SA-VCDs. We also found that the derived box profile parameters within a day tended to agree within the step resolution.

Overall, in 2008 there were 95 days were BrO of these days 61 of these days had above the detection limit, *d*SCD BrO at low elevation angles $> 3 \times 10^{13}$ molecules cm^{-2}. 49 of those 61 days resulted in measurements that passed the filter limits, 80% of the data.

3.2 Elevated viewing SA-VCD estimates and comparison to box profiles

We can compare the results from the full box profile fitting method to those derived from the simpler elevated viewing method. A simple correlation plot between the BrO calculated using box profile SA-VCD versus the elevated viewing $\text{SA-VCD}_{\text{EV}}$ resulted in slopes of 1.15 (r^2=0.956) and 1.11 (r^2=0.934) for 10° and 20° viewing elevations, respectively. This agreement between these two methods indicted that the box profile is a valid approximation of the atmosphere for the reported days and that the BrO observed is a surface associated layer.

3.3 Surface concentration estimates from box profile and horizon viewing methods

Vertical column densities were determined by the box profile method by simply dividing the SA-VCD by the best-fitted layer height to give a surface concentration of the trace gas. It is important to note that this conversion is highly dependent on the derived layer height parameter, as the height parameter is used both in the calculation of the SA-VCD and the concentration. In addition, the trace gas profile may be significantly more complex than the simple box profile, which would not be taken into account by this simple method. We can compare the surface trace gas concentration from the box profile method to the simpler horizon viewing method. Figure 7 shows a time series of the derived BrO concentration from both the box profile method and from the horizon viewing method applied to 2° elevation angle data. The horizon viewing method results in a slightly higher BrO concentration than the box profile method. A correlation plot resulted in a linear relationship of a slope of 1.04 with an r^2 of 0.90. This result indicates that the horizon viewing method is reasonable and could be used in the field to obtain an immediate estimate of the near-surface BrO concentration.

4 Conclusions

We outlined two methods to determine *d*SCDs using different Fraunhofer reference spectra, the DZ-MAXDOAS analysis, which employed a daily zenith reference and the LZ-MAXDOAS, which employed a local zenith reference. The DZ-MAXDOAS method allows fitting of twilight profiles to extract twice daily stratospheric SA-VCD estimates, but requires a secondary subtraction to give surface associated trace gas relevant *d*SCD observations. The LZ-MAXDOAS fitting procedure minimizes any stratospheric influences and provides the best data with the least instrumental error for analysis of surface associated trace gases.

We describe three rapid and easy-to-understand methods to analyze the MAXDOAS data. The box profile method arrives at the best surface-associated trace gas profile utilizing only two parameters, the box top height and the trace gas SA-VCD. This method also provides checks on the data and rejects data that have observations inconsistent with a simple box profile. For BrO during two months of 2008, approximately 80% of the data could be assigned an appropriate box profile, demonstrating the success of the method. The elevated viewing method estimates the SA-VCD of the trace gas by only using higher elevation viewing data and average airmass factors. It is shown that the elevated viewing method gives good agreement with the more advanced box profile method. The horizon viewing method estimates the pathlength from O_4 observations and then applies that pathlength to give an estimate of the surface concentration of the trace gas. It is shown that this method has good agreement with the box profile derived surface concentrations for BrO from the two-month data set.

We see these three simple methods as having a number of advantages over less general or more complex methods. The box model is applicable independent of time, method or trace gas species. This approach can be use during multiple campaigns and between many groups thereby aiding in intercomparison and validation studies. Second, this method makes a series of simple assumptions that result in two well-defined parameters, which can be compared to ancillary data. However, as this is a simple approximation of the atmospheric conditions, this model will not be appropriate for all observations. Therefore we applied a set of limits to quantify the validity of the simple vertical profile, and ensured that we accounted for the decreasing sensitivity of the MAXDOAS observations as the visibility decreases. We believe that this method also has a major advantage of being based on mathematical standard without the influence of a human observer, thereby guaranteeing that all data sets are treated in a uniform manor. Lastly, the results from this simple analysis can be used to check that a more advanced analysis (e.g. an optimal estimate inversion) is giving reasonable results.

Acknowledgement. We thank the National Science Foundation (NSF) for funding under grant (ARC-0612457) and the National Aeronautics and Space Administration (NASA), under grant (NNX09AB21G). We thank the Barrow Arctic Science Consortium (BASC) for logistical support in Barrow, Alaska. We acknowledge the use of and thank the authors of the TRACY-II radiation transfer model, developed by Thomas Wagner and Tim Deutschmann.

References

Afe, O. T., Richter, A., Sierk, B., Wittrock, F., and Burrows, J. P.: BrO emission from volcanoes: A survey using GOME and SCIAMACHY measurements, Geophys. Res. Lett., 31, L24113, doi:10.1029/2004GL020994, 2004.

Aliwell, S. R., Van Roozendael, M., Johnston, P. V., Richter, A., Wagner, T., Arlander, D. W., Burrows, J. P., Fish, D. J., Jones, R. L., Tørnkvist, K. K., Lambert, J.-C., Pfeilsticker, K., and Pundt, I.: Analysis for BrO in zenith-sky spectra: an intercomparison exercise for analysis improvement, J. Geophys. Res., 107(D14), 4199, doi:10.1029/2001JD000329, 2002.

Birch, K. P. and Downs, M. J.: An updated Edlén Equation for the refractive index of air, Metrologia, 30, 155–162, 1993.

Bogumil, K.: Temperature dependent absorption cross sections measured with the SCIAMACHY satellite spectrometer: http://www.iup.uni-bremen.de/gruppen/molspec/SCIA.html, last access: 7 August, 2009.

Carlson, D., Donohoue, D., Platt, U., and Simpson, W. R.: A low power automated MAX-DOAS instrument for the Arctic and other remote unmanned locations, Atmos. Meas. Tech., 3, 429–439, doi:10.5194/amt-3-429-2010, 2010.

Deutschmann, T. and Wagner, T.: TRACY-II manual 0.85, Institut für Umweltphysik der Universität Heidelberg, Heidelberg, 30 pp., 2007.

Dobson, G. M. B. and Harrison, D. N.: Measurements of the amounts of ozone in the Earth's atmosphere and its relation to other geophysical conditions, P. Roy. Soc. Lond. A, 110, 660–693, 1926.

Fayt, C. and Van Roozendael, M.: WinDoas 2.1 – Software User Manual, Belgian Institute for Space Aeronomy, Brussels, 91 pp., 2001.

Frieß, U., Monks, P. S., Remedios, J. J., Rozanov, A., Sinreich, R., Wagner, T., and Platt, U.: MAX-DOAS O_4 measurements: a new technique to derive information on atmospheric aerosols: 2. Modeling studies, J. Geophys. Res., 111, D14203, doi:10.1029/2005JD006618, 2006.

Greenblatt, G. D., Orlando, J. J., Burkholder, J. B., and Ravishankara, A. R.: Absorption measurements of oxygen between 330 and 1140 nm, J. Geophys. Res., 95, 18577–18582, 1990.

Hausmann, M. and Platt, U.: Spectroscopic measurement of bromine oxide and ozone in the high arctic during polar sunrise experiment 1992, J. Geophys. Res., 99, 25399–25413, 1994.

Hebestreit, K., Stutz, J., Rosen, D., Matveiv, V., Peleg, M., Luria, M., and Platt, U.: DOAS measurements of tropospheric bromine oxide in mid-latitudes, Science, 283, 55–57, 1999.

Heckel, A., Richter, A., Tarsu, T., Wittrock, F., Hak, C., Pundt, I., Junkermann, W., and Burrows, J. P.: MAX-DOAS measurements of formaldehyde in the Po-Valley, Atmos. Chem. Phys., 5, 909–918, doi:10.5194/acp-5-909-2005, 2005.

Hermans, C., Vandaele, A. C., and Carleer, M.: Absorption cross-section of atmospheric constituents: NO_2, O_2, and H_2O, Environ. Sci. Pollut. Res., 6, 151–158, 1999.

Hermans, C., Vandaele, A. C., Coquart, B., Jenouvrier, A., Merienne, M. F., Fally, S., Carleer, M., and Colin, R.: Absorption bands of O_2 and its collision-induced bands in the 30 000–7500 cm^{-1} wavenumber region, in: IRS 2000: Current Problems in Atmospheric Radiation, edited by: Smith, W. L. and Timofeyev, Y. M., A. Deepak, Hampton, VA, 639–642, 2001.

Hönninger, G. and Platt, U.: Observations of BrO and its vertical distribution during surface ozone depletion at Alert, Atmos. Environ., 36, 2481–2489, 2002.

Hönninger, G., von Friedeburg, C., and Platt, U.: Multi axis differential optical absorption spectroscopy (MAX-DOAS), Atmos. Chem. Phys., 4, 231–254, doi:10.5194/acp-4-231-2004, 2004a.

Hönninger, G., Leser, H., Sebastian, O., and Platt, U.: Ground-based measurements of halogen oxides at the Hudson Bay by active longpath DOAS and passive MAX-DOAS, Geophys. Res. Lett., 31, L04111, doi:10.1029/2003GL018982, 2004b.

Hönninger, G., Bobrowski, N., Palenque, E. R., Torrez, R., and Platt, U.: Reactive bromine and sulfur emissions at Salar de Uyuni, Bolivia, Geophys. Res. Lett., 31, L04101, doi:10.1029/2003GL018818, 2004c.

Knepp, T. N., Bottenheim, J., Carlsen, M., Carlson, D., Donohoue, D., Friederich, G., Matrai, P. A., Netcheva, S., Perovich, D. K., Santini, R., Shepson, P. B., Simpson, W., Valentic, T., Williams, C., and Wyss, P. J.: Development of an autonomous sea ice tethered buoy for the study of ocean-atmosphere-sea ice-snow pack interactions: the O-buoy, Atmos. Meas. Tech., 3, 249–261, doi:10.5194/amt-3-249-2010, 2010.

Kurucz, R. L., Furenlid, I., Brault, J., and Testerman, L.: Solar flux atlas from 296 nm to 1300 nm, Natl. Sol. Obs. Atlas 1, Harvard University, Cambridge, MA, 239 pp., 1984.

Lee, C., Richter, A., Lee, H., Kim, Y. J., Burrows, J. P., Lee, Y. G., and Choi, B. C.: Impact of transport of sulfur dioxide from the Asian continent on the air quality over Korea during May 2005, Atmos. Enivron., 42, 1461–1475, 2008.

Leigh, R. J., Corlett, G. K., Frieß, U., and Monks, P. S.: Spatially resolved measurements of nitrogen dioxide in an urban environment using concurrent multi-axis differential optical absorption spectroscopy, Atmos. Chem. Phys., 7, 4751–4762, doi:10.5194/acp-7-4751-2007, 2007.

Leser, H., Hönninger, G., and Platt, U.: MAX-DOAS measurements of BrO and NO_2 in the marine boundary layer, Geophys. Res. Lett., 30(10), 1537, doi:10.1029/2002GL015811, 2003.

Li, X., Brauers, T., Shao, M., Garland, R. M., Wagner, T., Deutschmann, T., and Wahner, A.: MAX-DOAS measurements in southern China: retrieval of aerosol extinctions and validation using ground-based in-situ data, Atmos. Chem. Phys., 10, 2079–2089, doi:10.5194/acp-10-2079-2010, 2010.

Long, C. A. and Ewing, G. E.: Spectroscopic investigation of van der Waals molecules, I. The infrared and visible spectra of $(O_2)_2$, J. Chem. Phys., 58, 4824, doi:10.1063/1.1679066, 1973.

Rodgers, C. D.: Retrieval of atmospheric temperature and composition from remote measurements of thermal radiation, Rev. Geophys., 14, 609–624, 1976.

Rozanov, A., Rozanov, V., Buchwitz, M., Kokhanovsky, A., and Burrows, J. P.: SCIATRAN 2.0 – a new radiative transfer model for geophysical applications in the 175–2400 nm spectral region, Adv. Space. Res., 36, 1015–1019, 2005.

Sinreich, R., Volkamer, R., Filsinger, F., Frieß, U., Kern, C., Platt, U., Sebastián, O., and Wagner, T.: MAX-DOAS detection of glyoxal during ICARTT 2004, Atmos. Chem. Phys., 7, 1293–1303, doi:10.5194/acp-7-1293-2007, 2007.

Sneep, M. and Ubachs, W.: Cavity ring-down measurements of the O_2-O_2 collision-induced absorption resonance at 477 nm at sub atmospheric pressures, J. Quant. Spectrosc. Ra., 78, 171–178, 2003.

Sneep, M., Ityaksov, D., Aben, I., Linnartz, H., and Ubachs, W.: Temperature-dependent cross sections of O_2–O_2 collision-induced absorption resonances at 477 and 577 nm, J. Quant. Spectrosc. Ra., 98, 405–424, 2006.

Vandaele, A. C., Hermans, C., Simon, P. C., Carleer, M., Colin, R., Fally, S., Merienne, M. F., Jenouvrier, A., and Coquart, B.: Measurements of the NO_2 absorption cross-section from 42 000 cm^{-1} to 10 000 cm^{-1} (238–1000 nm) at 220 K and 294 K, J. Quant. Spectrosc. Ra., 59, 171–184, 1998.

Wagner, T., Dix, B., von Friedeburg, C., Frieß, U., Sanghavi, S., Sinreich, R., and Platt, U.: MAX-DOAS O_4 measurements: A new technique to derive information on atmospheric aerosols – principles and information content, J. Geophys. Res., 109, D22205, doi:10.1029/2004JD004904, 2004.

Wagner, T., Burrows, J. P., Deutschmann, T., Dix, B., von Friedeburg, C., Frieß, U., Hendrick, F., Heue, K.-P., Irie, H., Iwabuchi, H., Kanaya, Y., Keller, J., McLinden, C. A., Oetjen, H., Palazzi, E., Petritoli, A., Platt, U., Postylyakov, O., Pukite, J., Richter, A., van Roozendael, M., Rozanov, A., Rozanov, V., Sinreich, R., Sanghavi, S., and Wittrock, F.: Comparison of box-air-mass-factors and radiances for Multiple-Axis Differential Optical Absorption Spectroscopy (MAX-DOAS) geometries calculated from different UV/visible radiative transfer models, Atmos. Chem. Phys., 7, 1809–1833, doi:10.5194/acp-7-1809-2007, 2007.

Wilmouth, D. M., Hanisco, T. F., Donahue, N. M., and Anderson, J. G.: Fourier transform ultraviolet spectroscopy of the $A(^2\Pi_{3/2})\leftarrow X(^2\Pi_{3/2})$ transition of BrO, J. Phys. Chem., 103, 8935–8944, 1999.

Wittrock, F., Müller, R., Richter, A., Bovensmann, H., and Burrows, J. P.: Measurements of iodine monoxide (IO) above Spitsbergen, Geophys. Res. Lett., 27, 1471–1474, 2000.

Wittrock, F., Oetjen, H., Richter, A., Fietkau, S., Medeke, T., Rozanov, A., and Burrows, J. P.: MAX-DOAS measurements of atmospheric trace gases in Ny-Ålesund – Radiative transfer studies and their application, Atmos. Chem. Phys., 4, 955–966, doi:10.5194/acp-4-955-2004, 2004.

Table 1. A detailed description of the two fitting procedures used in this paper, LZ-MAXDOAS and DZ-MAXDOAS. The two fits are based on the fitting procedures outlined in Aliwell et al. (2002) with up-date cross-sections and a slightly larger window, 346 nm to 364 nm.

<table>
<tr><th colspan="2">Method</th><th>DZ-MAXDOAS</th><th>LZ-MAXDOAS</th></tr>
<tr><td colspan="2">Fraunhofer reference</td><td>Daily solar noon zenith spectrum, $I_{0,\mathrm{DZ}}$ (λ)</td><td>Zenith spectrum collected with record, $I_{0,\mathrm{LZ}}$ (λ)</td></tr>
<tr><td colspan="2">Wavelength calibration</td><td>QDOAS calibration on solar noon reference</td><td>QDOAS calibration on zenith reference</td></tr>
<tr><td colspan="2">Window</td><td colspan="2">346 to 364 nm</td></tr>
<tr><td colspan="2">Solar flux spectrum</td><td colspan="2">Kitt Peak solar flux data (Kurucz et al., 1984), convert to vacuum, binned into 0.01 nm steps, and 5 point smoothed</td></tr>
<tr><td colspan="2">Instrument function</td><td colspan="2">Calculated from 334 nm mercury peak</td></tr>
<tr><td colspan="2">Ring</td><td colspan="2">Calculated in DOASIS from a clear sky day</td></tr>
<tr><td>Cross-sections</td><td>BrO</td><td colspan="2">(Wilmouth et al., 1999); Standard convolution</td></tr>
<tr><td></td><td>NO_2</td><td colspan="2">(Vandaele et al., 1998); Standard convolution</td></tr>
<tr><td></td><td>O_4</td><td colspan="2">(Hermans et al., 2001); Standard convolution</td></tr>
<tr><td></td><td>O_3 (273 K)</td><td colspan="2">(Bogumil, 2000); I_0 convolution</td></tr>
<tr><td></td><td>O_3 (223 K)</td><td>(Bogumil, 2000); I_0 convolution</td><td>Not included</td></tr>
</table>

Title Page
Abstract Introduction
Conclusions References
Tables Figures
◂◂ ▸▸
◂ ▸
Back Close
Full Screen / Esc
Printer-friendly Version
Interactive Discussion

Title Page
Abstract | Introduction
Conclusions | References
Tables | Figures
◀| |▶
◀ ▶
Back | Close
Full Screen / Esc
Printer-friendly Version
Interactive Discussion

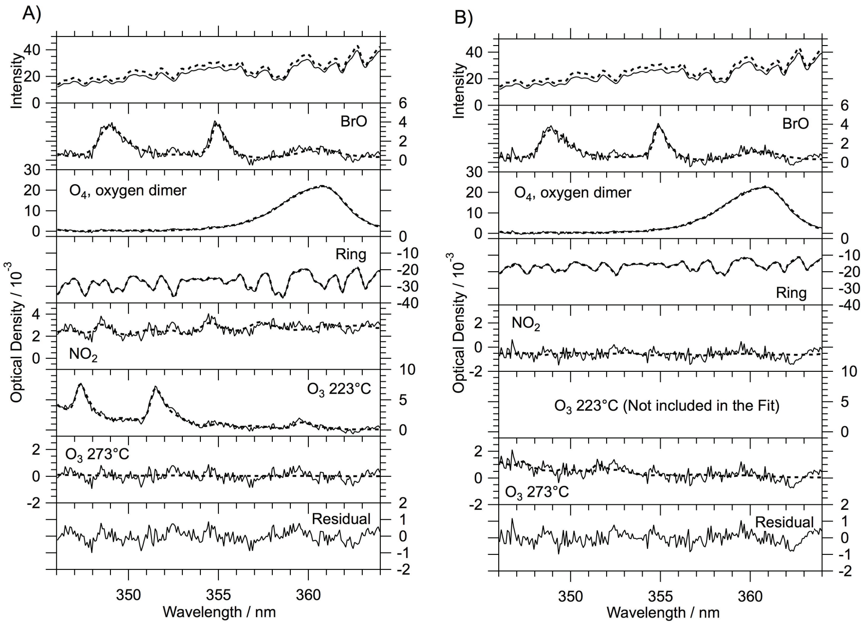

Fig. 1. Example of a spectral fit from Barrow, Alaska on 14 March 2008, 02:09 UTC (FDY = 74.1). The view elevation angle is 3° above the horizon and solar zenith angle (SZA) is 74°. In each panel, the solid line is the measurement spectrum and dotted line is the modeled partial fit, or the reference spectrum in the case of the top plot. Panel **(A)** is the DZ-MAXDOAS fitting with observed *d*SCDs (which are the fit coefficients) as follows: BrO: 4.05×10^{14} molecules cm^{-2}, O_4: 5.15×10^{43} molecules^2 cm^{-5}, NO_2: 5.76×10^{15} molecules cm^{-2}, O_3 at 273 K: 2.50×10^{17} molecules cm^{-2}, O_3 at 223 K: 2.17×10^{19} molecules cm^{-2}. Panel **(B)** is the LZ-MAXDOAS fitting with observed *d*SCDs as follows: BrO: 3.95×10^{14} molecules cm^{-2}, O_4: 5.28×10^{43} molecules^2 cm^{-5}, NO_2: -1.206×10^{15} molecules cm^{-2}, O_3 at 273 K: 2.85×10^{17} molecules cm^{-2}, O_3 at 223 K: not included in fit. The average RMS deviation of the residual spectrum from zero is 4.03×10^{-4}.

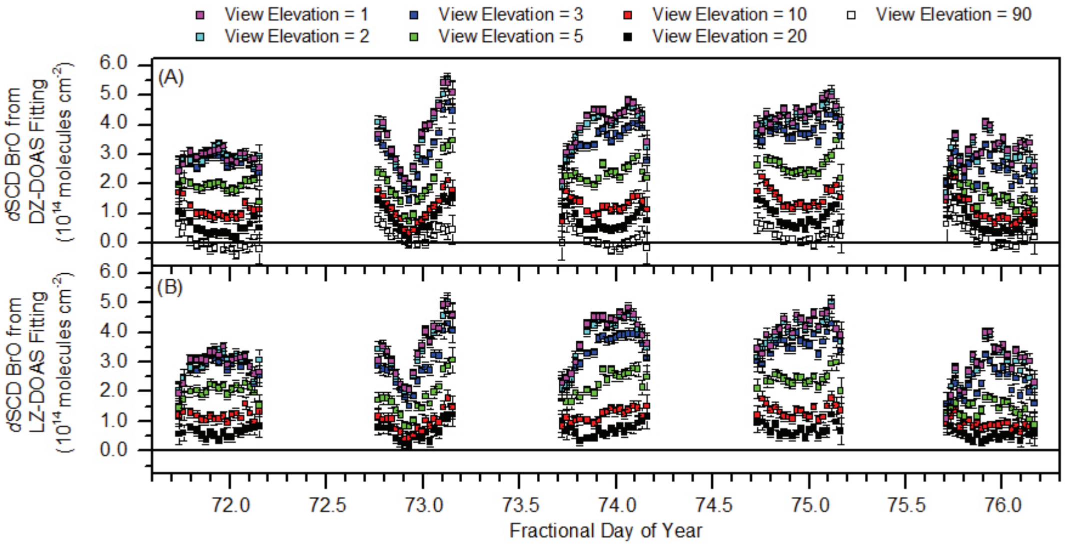

Fig. 2. Time series from 12 March thru 16 March 2008 (FDY = 72–77) of observed BrO *d*SCDs for DZ-MAXDOAS fitting – panel **(A)** and LZ-MAXDOAS fitting – panel **(B)**. The data is color coded by view elevation. Open black squares are the local solar zenith measurement, view elevation = 90°. Closed squares have view elevations of: black = 20°, red = 10°, green = 5°, blue = 3°, cyan = 2°, and pink = 1°.

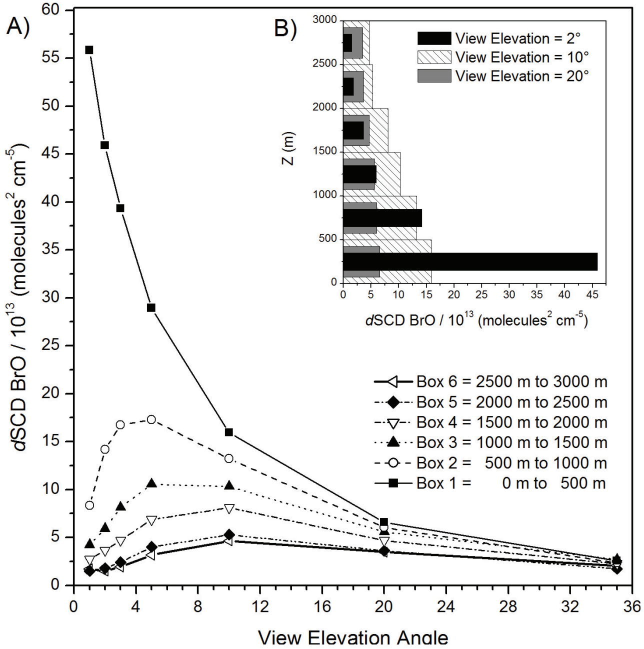

Fig. 3. Predicted BrO *d*SCD were determined from airmass factors calculated using 6 potential box profiles: Box 1 = 0 to 500 m (closed squares), Box 2 = 500 to 1000 m (open circles), Box 3=1000 to 1500 m (closed triangles), Box 4=1500 to 2000 m (open inverted triangles), Box 5 = 2000 to 2500 m (closed diamonds), Box 6 = 2500 to 3000 m (open rotated triangles). Each potential profile has a BrO SA-VCD of 3×10^{13} molecules^2 cm^{-5} and a visibility is 20 km. These were plotted against elevation angle in panel **(A)** to highlight the fact that if boundary layer BrO is present the lower elevation angles will have a strong signal which will dominate the *d*SCD profile. In panel **(B)** the relative sensitivities of each elevation are shown with height. Three view elevation angles are plotted; black = 2°, crosshatched = 10°, and grey = 20°. From this plot we see that the *d*SCDs at lower elevations are highly sensitive to the layer height while higher elevation *d*SCDs are less sensitive.

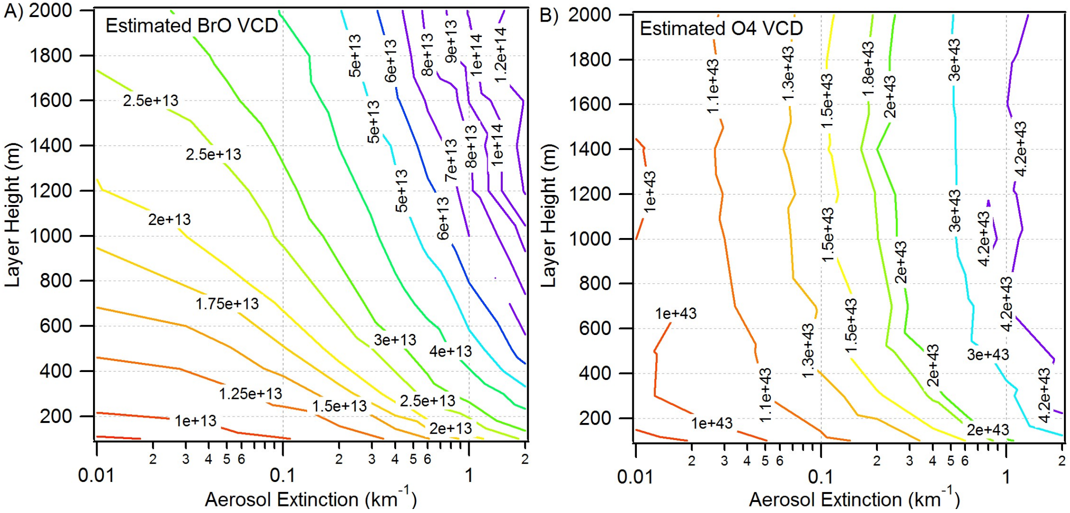

Fig. 4. Contour plots for the calculated SA-VCD$_{EST}$ for both BrO – panel **(A)** and O_4 – panel **(B)** on 16 March 2008, 22:00 UTC (FDY = 76.9). The solar zenith angle (SZA) was 73°. BrO SA-VCD contours range from 1×10^{13} (red) to 14×10^{13} (blue) molecules cm^{-2}. The O_4 SA-VCD contours vary from 1×10^{43} (red) to 4.2×10^{43} (purple) molecules^2 cm^{-5}; note that all box profiles which result in O_4 SA-VCDs above 1.3×10^{43} molecules^2 cm^{-5} are outside the O_4 fit limits.

Title Page
Abstract | Introduction
Conclusions | References
Tables | Figures
◀| |▶
◀ ▶
Back | Close
Full Screen / Esc
Printer-friendly Version
Interactive Discussion

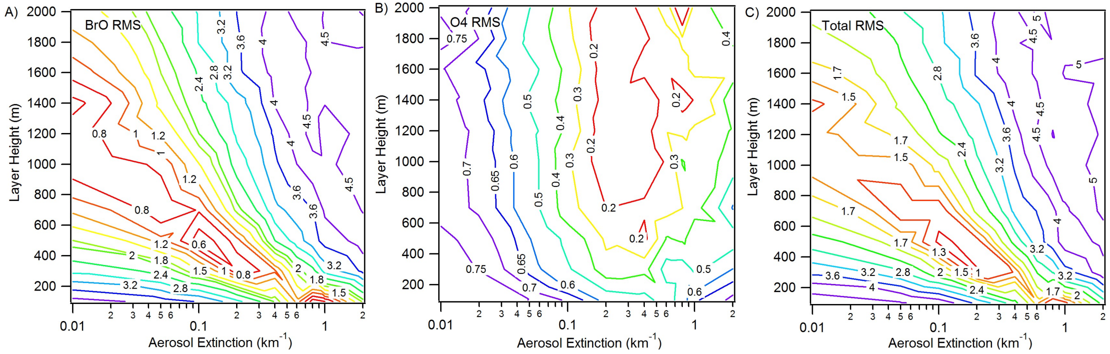

Fig. 5. Contour plots for the calculated RMS for BrO – panel **(A)**, O_4 – panel **(B)** and the total RMS, RMS BrO+RMS O_4, – panel **(C)** for 16 March 2008, 22:00 UTC (FDY = 76.9). The solar zenith angle (SZA) was 73°. Contour colors range from 0.2 (red) to 0.75 (purple) for O_4 and 0.4 (red) to 3 (purple) for the BrO and the total RMS. The best fit well at 0.2 km^{-1} (visibility of 5 km) and a layer height of 300 km, but the SA-VCD associated with these box model parameters are outside the O_4 limit with an O_4 SA-VCD of 1.5×10^{43} molecules^2 cm^{-5}. The minima does extend into values where the O_4 VCD is within the fit limits so the "best fit" box profile has parameters of 0.05 km^{-1} and a layer height of 700 km.

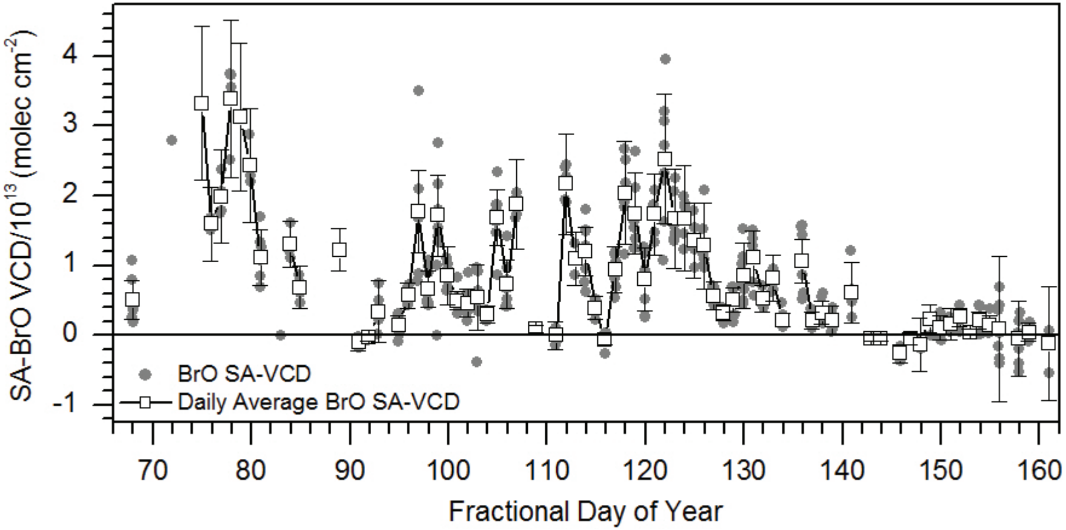

Fig. 6. A time series of the BrO SA-VCDs derived from the one box model from Barrow, AK from 6 March to 8 June 2008 (FDY = 67–162). This plot only includes data points which meet the fit limit: an upper limit of RMS deviation for the BrO SA-VCD and the O_4 SA-VCD of 1.5, as well as, a O_4 SA-VCD filter ($0.8\times10^{43}<O_4<1.3\times10^{43}$). The grey circles are the ~30 min data for the 2 h before and after solar noon. The open squares are the overall daily average.

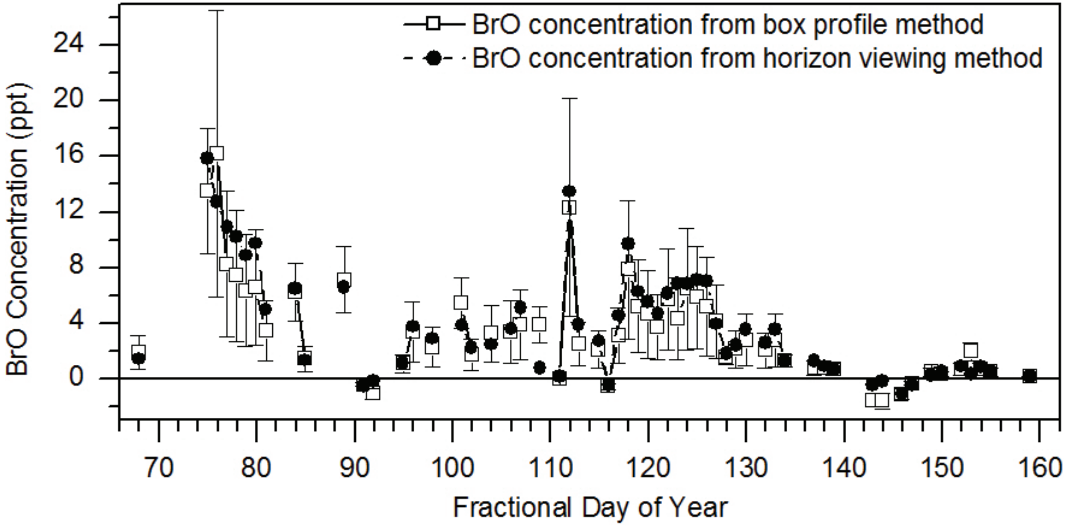

Fig. 7. A time series of the BrO concentration (ppt) from Barrow, AK from 6 March to 8 June 2008 (FDY = 67–167). The open squares were derived from the box profile method, while the closed circles were derived from the 2° horizon viewing method. We found that the 2° estimation method results in a slightly higher BrO concentration than the box model method; slope = 1.04 and $r^2 = 0.90$. However, as the BrO concentration determination has a significant error it we believe that the 2° horizon viewing method is a good, first order estimation of the BrO concentration that can be used in the field to obtain an immediate estimate of the BrO concentration.